

## ORIGINAL ARTICLE

# Design and Stability Analysis of a Super-Twisting Controller for a PS-FBC based Fuel Cell Module

Anderson J.L.\* | Moré J.J. | Puleston P.F.

<sup>1</sup>LEICI, Instituto de investigación en  
Electrónica, Control y Procesamiento de  
señales  
Facultad de Ingeniería UNLP - CONICET,  
La Plata, Argentina

**Correspondence**

Calle 48 y 116, CC 91 (1900), La Plata,  
Argentina. \*anderson.jorgeluis@gmail.com

**Summary**

Proton-Exchange Membrane Fuel Cells (PEM-FCs) have been established as a really promising technology, specially due to their high efficiency and scalability features, additionally to their low pollution emissions. In a typical topology, Fuel Cell Module (FCM) is usually integrated into a hybrid power system, where the FCM is designed to satisfy the main power requirements and reduce the current ripple at the Fuel Cell output. In this framework, the aim of this paper is to analyse and design a Sliding Mode Control (SMC) for a FCM based on an isolated Phase Shifted Full Bridge Converter (PS-FBC). This particular topology provides a high conversion ratio and attains a reduction of switching losses, which allow its application in low and medium power systems. From the control viewpoint, the proposed module represents a challenge due to the highly nonlinear behaviour and wide operation range of the FCM, together with system parameter uncertainties and perturbations. To solve these issues, a Second Order Sliding Mode Super-Twisting Algorithm (SOSM-STA) is proposed. As its main advantage, the STA reduces significantly the control chattering while preserving several features of conventional SMCs, such as robustness and finite time convergence. In order to analyse the zero dynamics stability, a Lyapunov study is proposed, taking advantage of its particular Liénard-type system structure. Finally, the designed algorithm is thoroughly analysed and validated by computer simulation on a commercial 10kW fuel cell module and compared to first order sliding mode control.

**KEYWORDS:**

Super-Twisting Algorithm, PEM Fuel Cell, Hybrid Power System

## 1 | INTRODUCTION

In recent years, the increasing concern about global warming has focused the world's interest on alternative sources of energy. In the latest years, due to high efficiency, reliability and clean energy, fuel cells have awoken as a promising technology for reducing pollution emissions.

A hydrogen based Fuel Cell (FC) is an electrochemical device which produces electricity through the oxidation of hydrogen, with water and heat as by-products. Different fuel cells exist depending on the electrolyte and the type of reaction involved. One of the most promising is the Proton-Exchange Membrane Fuel Cell (PEM-FC), which has enhanced special interest for transportation applications<sup>1</sup> and has also been considered for power system generation and portable applications (e.g.<sup>2,3</sup>). The

main advantages of the PEM-FC are its low operating temperature, compactness, reduced weight, scalability, high efficiency and high energy density. However, its high cost and relatively reduced lifetime remain as the main disadvantages of this fuel cell technology<sup>4</sup>.

From the electrical systems perspective, the fuel cells also present some drawbacks for their integration into a power system, mainly because of important nonlinearities and wide variations in their output voltage. In addition, due to a lack of bidirectional current flow, a slow dynamic response against load changes and the already mentioned wide voltage variations, the fuel cell needs to be integrated into a power conditioning system. Moreover, in order to satisfy the power demand of a changing load, it is indispensable to incorporate the fuel cell system into a hybrid power system.

Diverse topologies of hybrid power systems that also involve an Energy Storage System (ESS) are described in the literature<sup>5,6,7</sup>. The auxiliary ESS is usually designed to provide peak-load demand and to regulate the voltage of a common DC bus. In this way, the FC is normally connected to the bus of the hybrid system through a DC/DC converter (see Fig. 1). This converter must be able to operate efficiently under all FC module conditions, while ensuring low ripple at the FC output current and increasing its useful life.

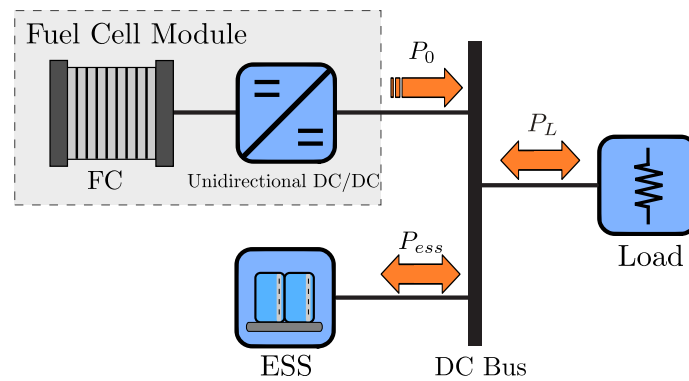


**FIGURE 1** Schematic diagram of a Fuel Cell Module as a part of a Hybrid Power System.

To fulfill such requirements, the family of converters known as Isolated DC/DC converters presents interesting features to deal with hybrid power systems that involve FC modules. In view of the low output voltage of the fuel cell, these converters provide a high conversion ratio through their high frequency transformer. Furthermore, the recent developments in planar magnetic technology led to cost, size and weight reduction, improving the performance of the overall system<sup>8,9</sup>. Particularly, the Phase-Shifted Full Bridge Converter (PS-FBC) diminishes switching stress, allowing its application in low and medium power systems<sup>10</sup>. In addition, the PS-FB converter is capable of using Zero Voltage Switching (ZVS) techniques to attain a reduction of switching losses<sup>11</sup>.

In this context, the control system plays a fundamental role. On account of the inherent nonlinearities of the FC and its power conditioning system, linear control techniques usually have low performance<sup>12</sup>, which is worsened due to its wide range of operation. Moreover, the existence of uncertainties and disturbances demands the utilization of a robust controller capable of ensuring stability and performance for such operation range. In the past, very satisfactory results have been obtained using Sliding Mode Control (SMC) for PS-FB Converters (e.g.<sup>13,14</sup>), but chattering effect remains as its main drawback.

Evolving from classic SMC, Second Order Sliding Mode (SOSM) has emerged as a powerful approach to mitigate chattering issues, with innovative contributions that continues to this day<sup>15,16,17,18,19</sup>. This kind of algorithms preserves conventional SMC's features of robustness and finite-time convergence, while providing chattering reduction. The presented chattering amelioration allows reducing losses and increases the FCM lifetime. Therefore, in this work a SOSM Super-Twisting Algorithm (STA) for a PS-FBC based Fuel Cell Module is analysed and developed. The STA controller allows its application directly to systems with relative degree one, as in the present topology, achieving a reduction of the chattering through its continuous control action. Also, the proposed STA has low computational complexity for online applications.

On the other hand, it has been widely reported in the literature<sup>20</sup> that, when a power system is designed to control electrical power delivered to a constant DC bus, its internal dynamics could present stability issues. Regarding this problem, eigenvalue analysis are commonly performed in the literature<sup>21,22,23</sup> to the study of microgrid applications with constant input voltage

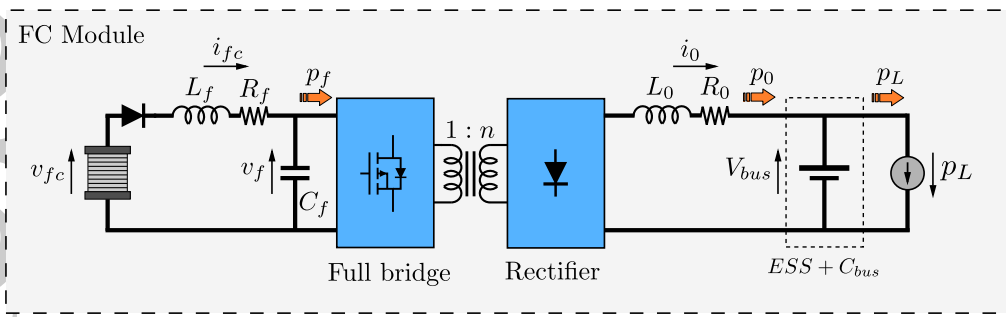


**FIGURE 2** Phase-Shifted Full Bridge Converter based FC Module

sources. However, these linearised analysis could not be sufficient for systems that involve fuel cells due to their high nonlinearity and wide voltage variation. Therefore, it becomes necessary to establish a general condition that guarantee the secure operation of the FCM, in all its range. For this reason, a Lyapunov study is proposed in this paper to analyse the nonlinear internal dynamics of the FCM. This study is performed taking advantage of its particular Liénard-type system structure, establishing a sufficient condition to achieve the control system stability.

The structure of the paper is organized as follows. In section 2, the electrical model of the PS-FBC based FCM, employed in the control analysis, is described. The design procedure of the proposed SOSM Super-Twisting Algorithm is presented and developed in section 3. In section 4 the zero dynamics of the control system are analysed by means of a Lyapunov approach, finding a sufficient condition to guarantee their stability. In section 5 the designed algorithm is thoroughly analysed and validated by computer simulation on a commercial 10kW fuel cell module and compared to first order sliding mode control. Finally, in section 6, the conclusions and future works are discussed.

## 2 | MODELLING OF THE FC MODULE

The Fuel Cell Module under study is considered to operate as the core of a Hybrid Power System, where an auxiliary ESS assists the FCM to supply the peak-load power and to regulate the bus voltage of a common DC bus, as was shown in Fig. 1. This system structure is capable of functioning over a wide operating range, satisfying abruptly variable electric loads like the ones present in electrical vehicles.

In this topology, the FC is connected to the DC link through a cascaded second-order filter and a dedicated DC/DC PS-FB Converter (see Fig. 2). The FCM is responsible for managing the main power required by the variable load, while safeguarding the FC integrity and increasing its lifetime.

In the remainder of this section the modelling of the PS-FBC based FCM is described.

### 2.1 | PEM Fuel Cell

As was mentioned earlier, PEM fuel cell voltage is a nonlinear function of the power load, as well as the temperature and pressure of the FC. The output voltage of an individual cell  $V_{cell}$  can be described, by considering its three most relevant losses, i.e.<sup>24</sup>

$$V_{cell} = E - \Delta V_{act} - \Delta V_{ohm} - \Delta V_{conc}$$

where  $E$  is the theoretical open circuit voltage of a hydrogen fuel cell, which highly depends on temperature and partial pressures.  $\Delta V_{act}$ ,  $\Delta V_{ohm}$  and  $\Delta V_{conc}$  are the activation, ohmic and concentration losses, respectively. Their effects are displayed in Fig 3 (for constant temperature and pressure).

At low current, there is a voltage drop due to the necessary energy to start the chemical reaction. These activation losses  $\Delta V_{act}$  can be described by the Tafel equation. The  $\Delta V_{ohm}$  are the losses due to electrical and ionic resistance of electrodes and electrolyte, resulting in a linear loss. Lastly, the  $\Delta V_{conc}$  represents losses due to changes in reactant concentrations, which produce a reduction in their partial pressures. This voltage drop can be described empirically by an exponential law, leading to an important loss at high current.

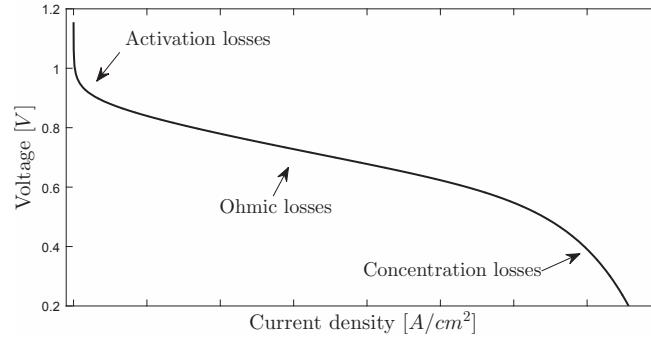


**FIGURE 3** A typical voltage-current density curve of an individual PEM fuel cell.

Assuming regulated temperatures and partial pressures, an empirical model that provides a very good fit to experimental results of real FC stacks, is<sup>24</sup>

$$v_{fc}(i_{fc}) = N_{stack} \cdot E_{nl} - v_{act}(i_{fc}) - v_{conc}(i_{fc}) - R_{ohm} \cdot i_{fc} \quad (1)$$

Where the overvoltage due to activation and concentration losses,  $v_{act}$  and  $v_{conc}$  respectively, can be described as nonlinear functions of the fuel cell current:

$$v_{act}(i_{fc}) = N_{stack} \cdot A_t \cdot \ln(i_{fc}), \quad (2)$$

$$v_{conc}(i_{fc}) = N_{stack} \cdot m \cdot \exp(n \cdot i_{fc}) \quad (3)$$

with  $N_{stack}$  the number of cells,  $E_{nl}$  the open circuit voltage,  $A_t$  the slope of the Tafel equation, and  $m$  and  $n$  empirical coefficients. The stack resistance in the ohmic losses as the linear term, is given by:

$$R_{ohm} = N_{stack} \cdot r_{ohm}, \quad (4)$$

with  $r_{ohm}$  the resistance of a single cell. The electrical static model described in (1) has been successfully applied to the power system analysis that involves FCs, and it is extensively used in the literature<sup>25,26,27</sup>. For these reasons, the presented static model is used in the following study to design the proposed system controller. Then, in the result section 5, the analysis is validated through an extended model that includes the double layer effect of FCs.

## 2.2 | Phase Shifted Full Bridge Converter (PS-FBC)

The main characteristic of the PS-FBC is to use an intermediate AC stage to obtain a high conversion ratio through a High Frequency Transformer (HFT). This feature is fundamental for low-voltage input applications, avoiding the converter to operate with a large duty cycle. On account of its switch stress reduction and low switching losses, converters based on soft-switched modulation techniques, such as Phase-Shifted, are particularly well-suited to operate in medium-power applications.

As shown in Fig. 2, the PS-FBC consists of a single-phase, full bridge inverter connected to the primary winding of the HFT. Each inverter's leg generates a square-wave signal, working with a 50% duty cycle. As a result of the phase shift  $\phi$  between both legs, a 3-level signal is produced over the HFT<sup>11</sup>. The secondary winding of the transformer is connected to a diode rectifier, linked to the common DC bus by the inductor  $L_0$ .

In addition, a second order low-pass filter is included between the fuel cell and the PS-FBC to allow a reduced ripple current at the FC output.

Under the following assumptions:

- The HFT is ideal,
- Only output and filter inductor losses are considered, neglecting switches and diode losses,
- The output current  $i_0$  never reaches a zero value, and
- The bus voltage is perfectly regulated by the ESS to a constant value, equal to  $V_{bus}$ ,

the model of the FCM, presented in Fig. 1, is<sup>28</sup>:

$$\begin{cases} L_f \cdot \frac{d\bar{i}_{fc}}{dt} &= -\bar{i}_{fc} \cdot R_f - \bar{v}_f + v_{fc(\bar{i}_{fc})} \\ C_f \cdot \frac{d\bar{v}_f}{dt} &= \bar{i}_{fc} - \bar{i}_0 \cdot n \cdot u(t) \\ L_0 \cdot \frac{d\bar{i}_0}{dt} &= -\bar{i}_0 \cdot R_0 - V_{bus} + n \cdot \bar{v}_f \cdot u(t) \end{cases} \quad (5)$$

where the state  $\bar{i}_{fc}$  is the average current in the fuel cell,  $\bar{v}_f$  is the voltage across the input filter capacitor and  $\bar{i}_0$  is the current delivered to the DC bus. Additionally,  $u(t) = \frac{\phi(t)}{\pi}$  is the normalized phase shift or duty cycle, with  $0 < u_{min} < u(t) < 1$ . The  $u_{min}$  parameter is chosen in order to limit the operating range of the PS-FBC, avoiding discontinuous conduction mode. The last assumption implies that the ESS and the bus capacitor are viewed by the FCM as a regulated voltage source (see Fig. 2).

The system described by (5) is a control affine nonlinear system, i.e. it can be rewritten as:

$$\dot{x} = f_{(x)} + g_{(x)} \cdot u(t) \quad (6)$$

where

$$x = [x_1 \ x_2 \ x_3]' = [\bar{i}_{fc} \ \bar{v}_f \ \bar{i}_0]'$$

and

$$f_{(x)} = \begin{bmatrix} -\frac{R_f}{L_f} \cdot x_1 - \frac{1}{L_f} \cdot x_2 + \frac{v_{fc(x_1)}}{L_f} \\ \frac{1}{C_f} \cdot x_1 \\ -\frac{R_0}{L_0} \cdot x_3 - \frac{V_{bus}}{L_0} \end{bmatrix}, \quad (8)$$

$$g_{(x)} = \begin{bmatrix} 0 \\ -\frac{n}{C_f} \cdot x_3 \\ \frac{n}{L_0} \cdot x_2 \end{bmatrix}. \quad (9)$$

### 3 | DESIGN OF THE SOSM CONTROLLER FOR THE FCM

In this section, the design of the second order SMC Super-Twisting algorithm for the FCM is developed. The controller is intended to satisfy the tracking of a continuous FCM power reference  $p_{0r}$ , provided by an external supervisory control (the latter is not presented in this work, see e.g.<sup>29,30</sup>). This power reference is a smooth signal specifically designed to deliver the average load power, avoiding abrupt variations of the FC current. Thence, the control objective can be written, by means of the SMC theory, as

$$\sigma_{(x,t)} = V_{bus} \cdot x_3 - p_{0r(t)}, \quad (10)$$

where  $\sigma$  is a smooth function, usually called the *sliding variable*. Therefore, the objective is accomplished when the control strategy steers and maintains the sliding variable  $\sigma$  and its first derivative  $\dot{\sigma}$  to zero, i.e. when the system reaches and remains on the *sliding manifold*

$$\mathcal{S} = \{\forall x \in \mathbb{R}^3 : \sigma_{(x,t)} = \dot{\sigma}_{(x,t)} = 0\}. \quad (11)$$

Taking advantage of the control affine structure and the relative degree one of  $\sigma$  with respect to the control action  $u$ , the expression of  $\dot{\sigma}$  and  $\ddot{\sigma}$  can be easily obtained from (6)-(10) as

$$\dot{\sigma}_{(x,t)} = \Phi_{(x,t)} + \Gamma_{(x)} \cdot u(t) \quad (12)$$

$$\ddot{\sigma}_{(x,u,t)} = \varphi_{(x,u,t)} + \Gamma_{(x)} \cdot \dot{u}(t) \quad (13)$$

with

$$\Phi_{(x,t)} = \frac{d\sigma_{(x,t)}}{dx} \cdot f_{(x)} - \dot{p}_{0r(t)}, \quad (14)$$

$$\Gamma(x) = \frac{d\sigma_{(x,t)}}{dx} \cdot g_{(x)} \quad (15)$$

and

$$\varphi_{(x,u,t)} = \dot{\Phi}_{(x,t)} + \dot{\Gamma}_{(x)} \cdot u_{(t)}. \quad (16)$$

The SOSM design procedure implies bounding functions  $\varphi$  and  $\Gamma$  of the second time derivative  $\ddot{\sigma}$ <sup>31</sup>.

### 3.1 | SOSM Super-Twisting algorithm with feedforward action

To track the desired power reference, a two terms controller is proposed. The first term is a direct feedforward action  $u_{ff}$  which is designed to steer the system near to the desired operation region  $\sigma_{(x,t)} = 0$ , but it is not capable of dealing with uncertainties and disturbances. The second term is a SOSM based control action,  $u_{st}$ , which provides robust convergence to the sliding manifold  $S$  in finite time. Therefore, the proposed control action  $u$  is written as

$$u_{(x,t)} = u_{ff(x,t)} + u_{st(x,t)}. \quad (17)$$

The feedforward action  $u_{ff}$  is obtained considering the nominal system (see Fig. 2) with no uncertainties. It leads to

$$u_{ff(x,t)} = \frac{i_{0r(t)} \cdot R_0 + V_{bus}}{n \cdot x_2} \quad (18)$$

where the FCM current reference is

$$i_{0r(t)} = \frac{p_{0r(t)}}{V_{bus}}. \quad (19)$$

Next, to design the SOSM term,  $u_{st}$ , it is necessary to include the effect of the feedforward  $u_{ff}$  into (12)-(13), by substituting the proposed control (17) into (12). It follows that  $\dot{\sigma}$  can be rewritten as:

$$\dot{\sigma}_{(x,t)} = \Phi'_{(x,t)} + \Gamma_{(x)} \cdot u_{st(x,t)} \quad (20)$$

with

$$\begin{aligned} \Phi'_{(x,t)} &= \Phi_{(x,t)} + \Gamma_{(x)} \cdot u_{ff(x,t)} \\ &= -\frac{R_0}{L_0} \cdot V_{bus} \cdot (x_3 - i_{0r(t)}) - \dot{p}_{0r(t)}, \end{aligned} \quad (21)$$

$$\Gamma_{(x)} = \frac{n}{L_0} \cdot x_2 \cdot V_{bus}. \quad (22)$$

Similarly,  $\ddot{\sigma}$  is rewritten as:

$$\ddot{\sigma}_{(x,u,t)} = \varphi'_{(x,u,t)} + \Gamma_{(x)} \cdot \dot{u}_{st(t)} \quad (23)$$

where

$$\varphi'_{(x,u,t)} = \dot{\Phi}'_{(x,t)} + \dot{\Gamma}_{(x)} \cdot u_{st(t)}. \quad (24)$$

Note that the above equation is quite similar to (13) and its derivation is omitted for brevity, but it can be straightforwardly computed from the FCM equations.

It can be demonstrated<sup>32</sup> that, if there exist positive constants  $C$ ,  $K_m$  and  $K_M$  such that

$$|\varphi'_{(x,u,t)}| \leq C \text{ and } 0 < K_m \leq \Gamma_{(x)} \leq K_M, \quad (25)$$

a robust control action  $u_{st}$  which leads and maintains the system trajectories onto  $S$  in finite time is given by the SOSM Super-Twisting algorithm (see Fig. 4):

$$u_{st(x,t)} = -\lambda \cdot |\sigma_{(x,t)}|^{1/2} \cdot \text{sign}(\sigma_{(x,t)}) + \omega \quad (26)$$

$$\dot{\omega} = -\alpha \cdot \text{sign}(\sigma_{(x,t)}). \quad (27)$$

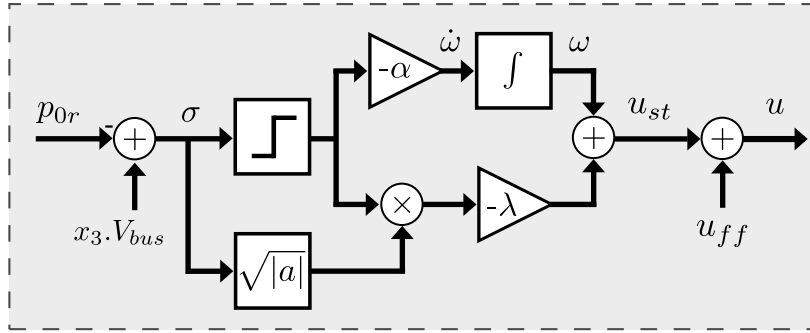


FIGURE 4 Scheme of the proposed control  $u = u_{ff} + u_{st}$ .

To guarantee this finite robust convergence of the algorithm, the controller parameters  $\alpha$  and  $\lambda$  must be chosen to satisfy:

$$\alpha > \frac{C}{K_m} \quad (28)$$

$$\lambda^2 > \frac{2}{K_m^2} \frac{(K_m \alpha + C)^2}{(K_m \alpha - C)}. \quad (29)$$

The latter bounds are only a sufficient condition for the algorithm convergence, and can be adjusted in order to improve the reduction of chattering.

### 3.2 | Bounding of $\varphi'$ and $\Gamma$ functions

From the bounds defined in (25), it is possible to find the controller parameters  $\alpha$  and  $\lambda$  that ensure reaching the system trajectories onto  $S$ . In order to guarantee the control robustness, the positive constants  $C$ ,  $K_m$  and  $K_M$  must be computed considering the uncertainty of the system model and perturbations. For this work, a PS-FBC parameters variation of  $\pm 20\%$  and a bus voltage variation of  $\pm 5\%$  have been considered. Within those ranges of variations, the searched system bounds are basically defined by the worst-case combination of parameter uncertainties.

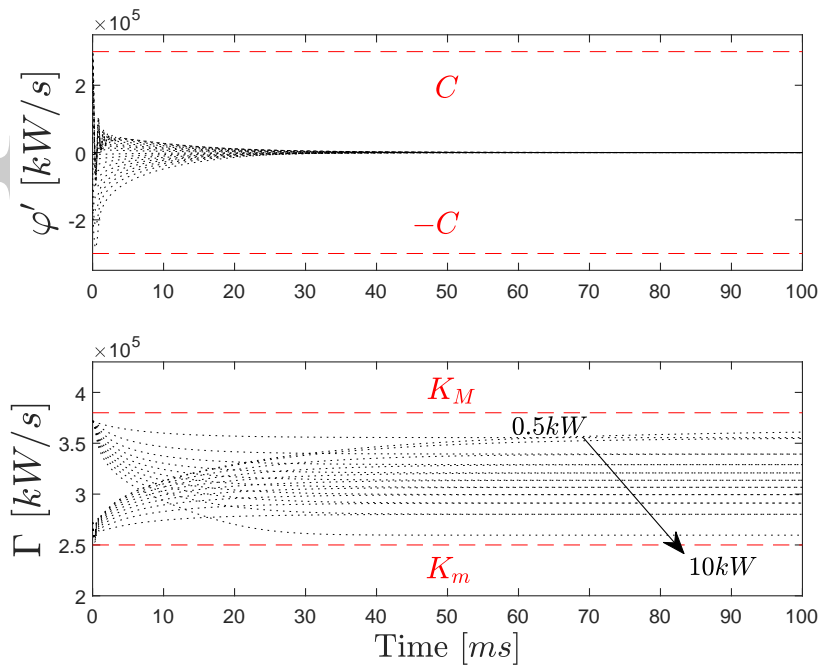


FIGURE 5  $\varphi'$  and  $\Gamma$  functions evaluated for diverse system trajectories.

The expression of  $\varphi'$  can be obtained from (10)-(16), resulting in a quite complex equation. Bounding this expression analytically, usually, is an arduous procedure which leads to very conservative bounds. For this reason, in the present work, the constants  $C$ ,  $K_m$  and  $K_M$  have been obtained using a numerical approach.

To illustrate this numerical procedure, Fig. 5 shows one of the sets of functions  $\varphi'$  and  $\Gamma$  that have been utilized for the practical tuning. The trajectories have been generated considering abrupt variations of  $u_{st}$ , which lead the system from the nominal power operation ( $\sim 10kW$ ) to a low power operation ( $\sim 0.5kW$ ), and vice versa.

After thorough simulation trials and analysis, where the system is evaluated taking into account the parameter variations previously mentioned, the desired bounds are determined. It should be noted that in practice, even though numerically obtained, the controller parameters  $\alpha$  and  $\lambda$  established by (28)-(29) should be iteratively adjusted in order to attain the desired robustness and chattering properties.

#### 4 | LYAPUNOV ZERO DYNAMICS ANALYSIS BASED ON A LIÉNARD APPROACH

In addition to the reachability condition imposed by (28)-(29), the system dynamics over the sliding manifold  $S$ , i.e. the Zero Dynamics (ZD), should be analysed to guarantee the control stability. In this way, it was identified that the particular ZD of the system can be reworked into a Liénard-type form<sup>33</sup>. This assists us to find a suitable energy-like Lyapunov function and, consequently, a stability condition for the Fuel Cell Module.

To this aim, the continuous control action  $u_{st}^{eq}$  required to maintain the system confined in the Sliding Surface  $S$  is obtained as<sup>34</sup>:

$$u_{st(x,t)}^{eq} = -\frac{\Phi'_{(x,t)}}{\Gamma_{(x)}} \Big|_{\sigma_{(x,t)}=0} = \frac{L_0}{n \cdot V_{bus}} \cdot \dot{p}_{0r(t)} \cdot \frac{1}{x_2}. \quad (30)$$

So, the Zero Dynamics are computed by substituting the proposed control action (17) into the system equations (6)-(9), taking into account  $u_{st}^{eq}$  and the condition  $\sigma_{(x,t)} = 0$ . It follows that the ZD system results in:

$$\begin{cases} L_f \cdot \dot{x}_1 = -x_2 - R_f \cdot x_1 + v_{fc(x_1)} \\ C_f \cdot \dot{x}_2 = x_1 - p_f(t) \frac{1}{x_2} \end{cases} \quad (31)$$

where  $p_f(t) = R_0 \cdot i_{0r(t)}^2 + L_0 \cdot i_{0r(t)} \cdot \dot{i}_{0r(t)} + p_{0r(t)}$  represents the instantaneous power at the FCM output.

As was previously stated, the variation of the external FCM power reference  $p_{0r}$  is in practice (see Sec. 5) much slower than the electrical response of the input filter (fast power variations are responsibility of the Energy Storage System, typically designed to provide peak load demand). Then, the first derivative of  $p_{0r}$  and of  $i_{0r}$  are negligible compared to the filter time constant thus, for the ZD analysis, the FCM power output  $p_f$  can be considered as:

$$p_f(t) \approx R_0 \cdot I_{0r}^2 + P_{0r} = R_0 \cdot \frac{P_{0r}^2}{V_{bus}^2} + P_{0r} = P_f \quad (32)$$

In this framework, the equivalent electrical circuit for the ZD is displayed in Fig. 6.

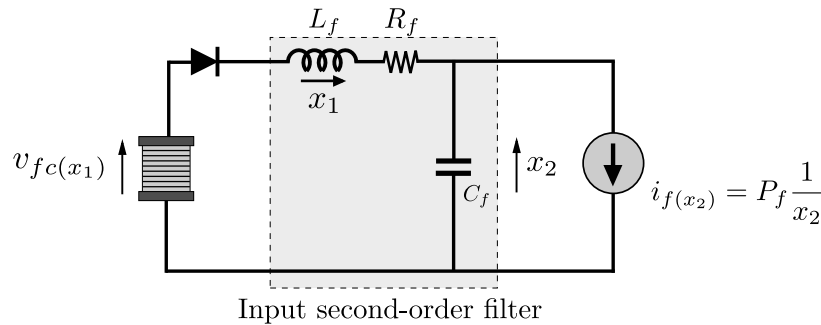


FIGURE 6 Equivalent electrical circuit of the zero dynamics.



The resulting electrical circuit presents stability issues, which have been extensively addressed in the literature for the particular case of a constant input voltage source<sup>22</sup>. These issues worsen in the studied case, because of the input voltage variations due to the fuel cell as system source. So, it becomes necessary to go into an in-depth analysis to establish a comprehensive condition, which guarantees the system stability over a wide range of operation. To this aim, in the following study, a parametrization of the fuel cell characteristic is developed, rewriting the fuel cell voltage and its equivalent losses as functions of the different operation point throughout its range. Using a Taylor approach in the neighborhood of each one of these points, the parametrization gives:

$$v_{fc}(x_1) = v_{fc}(x_1^0) + \left. \frac{\partial v_{fc}}{\partial x_1} \right|_{x_1^0} \cdot (x_1 - x_1^0) + H.O.T. \quad (33)$$

$$\approx v_{fc}(x_1^0) + \left. \frac{\partial v_{fc}}{\partial x_1} \right|_{x_1^0} \cdot (x_1 - x_1^0) \quad (34)$$

where  $x_1^0$  is the equilibrium inductor current, for the admissible reference power values  $p_{0r}$ .

The above considerations lead to the following expression for the Zero Dynamics:

$$\begin{cases} L_f \cdot \dot{x}_1 = -x_2 - R(x_2) \cdot x_1 + V_{fc}(x_2) \\ C_f \cdot \dot{x}_2 = x_1 - i_f(x_2) \end{cases} \quad (35)$$

where

$$R(x_2^0) = R_f - \left. \frac{\partial v_{fc}}{\partial x_1} \right|_{i_f(x_2^0)} \quad (36)$$

and

$$V_{fc}(x_2^0) = v_{fc}(i_f(x_2^0)) - \left. \frac{\partial v_{fc}}{\partial x_1} \right|_{i_f(x_2^0)} \cdot i_f(x_2^0) \quad (37)$$

with

$$i_f(x_2) = P_f \frac{1}{x_2} \quad (38)$$

As it can be seen, the parametrized losses  $R(x_2^0)$  and FC voltage  $V_{fc}(x_2^0)$  need to be computed for each operation point, defined by the reference power  $p_{0r}$ . This parametrization will help to find a valid condition for the nonlinear FC operation range. The equilibrium point determined by the current  $x_1^0$  and voltage  $x_2^0$ , corresponding to the state variables  $x_1$  and  $x_2$ , respectively, are obtained by

$$x_1^0 = i_f(x_2^0), \quad (39)$$

with  $x_2^0$  a solution of the equation

$$v_{fc}(i_f(x_2^0)) = R_f \cdot i_f(x_2^0) + x_2^0. \quad (40)$$

The dynamic system (35) has two equilibrium points, but just the equilibrium voltage  $x_2^0$  which is closer to the fuel cell voltage has physical meaning and is considered in the analysis. The system states can be redefined shifting the equilibrium point to the origin as

$$\bar{x}_1 = x_1 - i_f(x_2^0) \quad (41)$$

$$\bar{x}_2 = x_2 - x_2^0, \quad (42)$$

leading to the transformed system form:

$$\begin{cases} \dot{\bar{x}}_1 = -\frac{R(x_2^0)}{L_f} \bar{x}_1 - \frac{1}{L_f} \bar{x}_2 \\ \dot{\bar{x}}_2 = \frac{\bar{x}_1}{C_f} - \frac{1}{C_f} \{i_f(\bar{x}_2 + x_2^0) - i_f(x_2^0)\}. \end{cases} \quad (43)$$

Finally, applying the linear transformation

$$z_1 = \frac{1}{C_f} \bar{x}_1 + \frac{R(x_2^0)}{L_f} \bar{x}_2 \quad (44)$$

$$z_2 = \bar{x}_2, \quad (45)$$

we obtain the Liénard-type system

$$\dot{z}_1 = -g(z_2) \quad (46)$$

$$\dot{z}_2 = z_1 - F(z_2) \quad (47)$$

where

$$F(z_2) = \frac{R(x_2^0)}{L_f} \cdot z_2 + \frac{1}{C_f} \cdot \{i_f(z_2 + x_2^0) - i_f(x_2^0)\} \quad (48)$$

$$g(z_2) = \frac{1}{L_f C_f} \cdot z_2 + \frac{R(x_2^0)}{L_f C_f} \{i_f(z_2 + x_2^0) - i_f(x_2^0)\}. \quad (49)$$

Due to the above functions satisfy  $g(0) = F(0) = 0$ , the energy-like Lyapunov function of the transformed states  $z_1$  and  $z_2$ ,

$$V(z_1, z_2) = \frac{1}{2} \cdot z_1^2 + \mathcal{G}(z_2), \text{ with } \mathcal{G}(z_2) = \int_0^{z_2} g(\xi) d\xi \quad (50)$$

is locally positive-definite if  $g(z_2)$  satisfies the following condition

$$z_2 \cdot g(z_2) > 0, \quad (51)$$

for some interval

$$\mathcal{Z} = \{z_2 \in \mathbb{R} - \{0\} : \underline{z}_2 < z < \bar{z}_2; \underline{z}_2 < 0, \bar{z}_2 > 0\}. \quad (52)$$

The first derivative of  $V$  is equal to

$$\dot{V}(z_1, z_2) = -g(z_2) \cdot F(z_2) \quad (53)$$

which is locally negative-definite if  $g(z_2)F(z_2) > 0$ .

Moreover, if condition (51) is satisfied, it follows that

$$\begin{aligned} g(z_2) \cdot F(z_2) > 0 &\Rightarrow g(z_2)^2 \cdot z_2 \cdot F(z_2) > 0 \\ &\Leftrightarrow z_2 \cdot F(z_2) > 0. \end{aligned} \quad (54)$$

From equations (48)-(49) and conditions (51) and (54), it can be easily shown that a sufficient condition for the local system stability, as function of the original state variable  $x_2$ , is determined by

$$G_0(x_2^0, x_2) < \min \{G_{fc}(x_2^0), G_{lc}(x_2^0)\} \quad (55)$$

where the output conductance  $G_0$  is equal to

$$G_0(x_2^0, x_2) = \frac{i_f(x_2) - i_f(x_2^0)}{x_2^0 - x_2} \quad (56)$$

and the fuel cell conductance  $G_{fc}$  and the filter conductance  $G_{lc}$ , respectively, are

$$G_{fc}(x_2^0) = \frac{1}{R(x_2^0)} \quad \text{and} \quad G_{lc}(x_2^0) = \frac{C_f}{L_f} R(x_2^0). \quad (57)$$

The local stability condition (55) makes possible to construct a conductance diagram as function of the capacitor voltage  $x_2$ , taking into account different operation points (i.e. different values of  $P_f$ ). Fig. 7 shows a graphical representation of this condition, establishing a Stability Region (white area) where the ZD stability is locally guaranteed.

The Stability Region is delimited by the fuel cell  $G_{fc}$  and the filter  $G_{lc}$  conductances. To contemplate parameter variations and modelling errors, safe bounds of %20 has been considered for both  $G_{lc}$  and  $G_{fc}$  (the corresponding curves are depicted in red and blue, respectively, in Fig. 7). In this way, the output conductance at steady state,  $G_0(x_2^0, x_2^0)$ , remains inside this region, setting a secured voltage range for the filter capacitor.

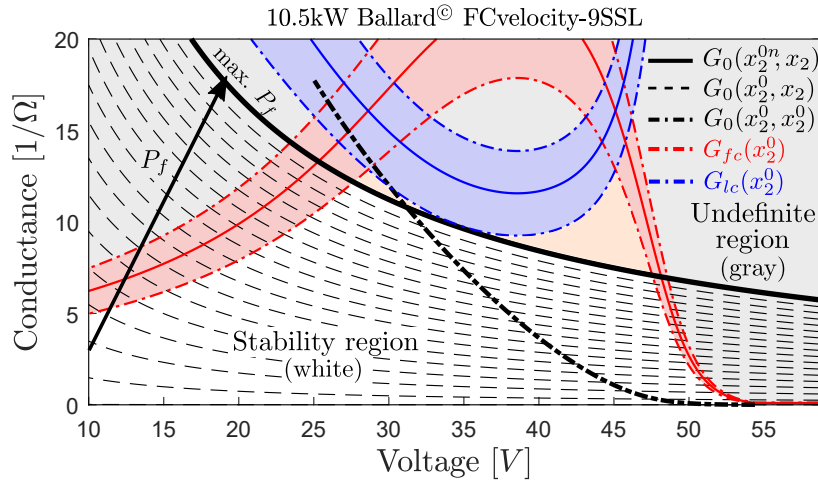


**FIGURE 7** Conductance diagram of the 10.5kW Ballard<sup>®</sup> fuel cell proposed to analyse the ZD dynamics stability.

## 5 | SIMULATION RESULTS

In this section, the performance of the designed SOSM-STA controller is assessed on a 10kW FCM. To evaluate the robustness of the proposed method under realistic operating conditions, a higher order model of the Hybrid Power System is used for the simulations (see Fig. 8), incorporating system model disturbances, uncertainties and dynamics unmodelled during the design procedures. For the latter, the double layer phenomenon of FCs is taken into consideration for the simulation model<sup>35</sup>, through the insertion of the capacitor  $C_{dl}$  connected in parallel with activation and concentration losses. In addition, a dynamic model for the ESS was assumed, comprising supercapacitors and a typical PI controlled Boost Converter (see Appendix).

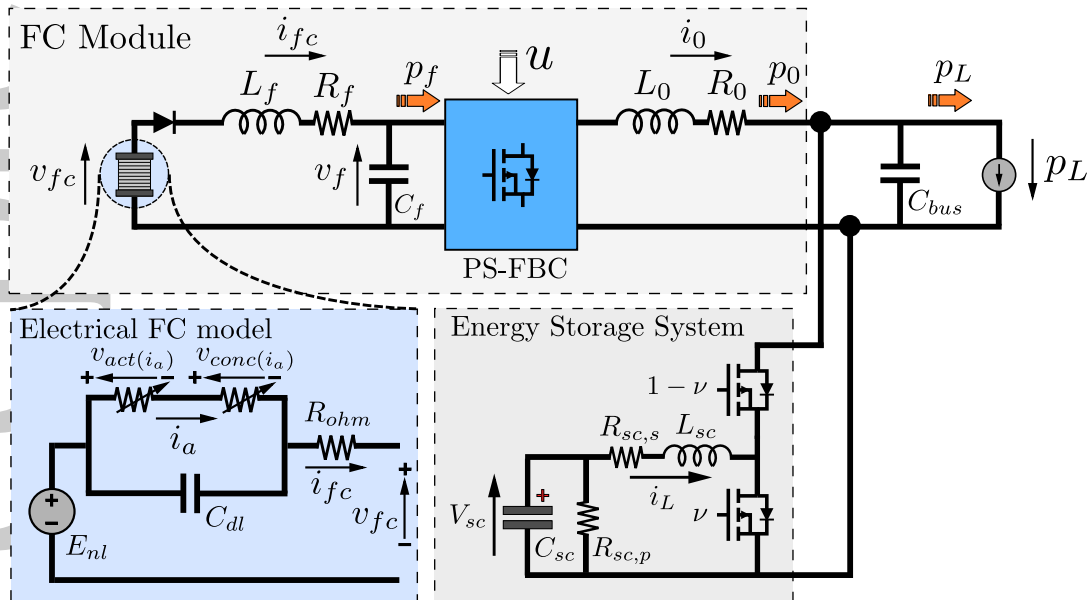


**FIGURE 8** Electrical model of the Hybrid Power System employed in the FCM validation.

The modeled FC is a Ballard FCvelocity-9SSL with a rated power of 10.5kW. Eq. (1) has been fitted to the FC polarization curve<sup>36</sup>, considering a nominal DC voltage of 35V at 300A. The HPS parameters employed in the simulations are presented in Table 1. The table also presents the controller parameters obtained through the procedure described in section 3.2. As was

explained there, up to 20% system parameters uncertainties have been considered for the controller design. To assess the control system under adverse conditions, the following simulations have been conducted assuming the worst-case scenario regarding parameters uncertainties.

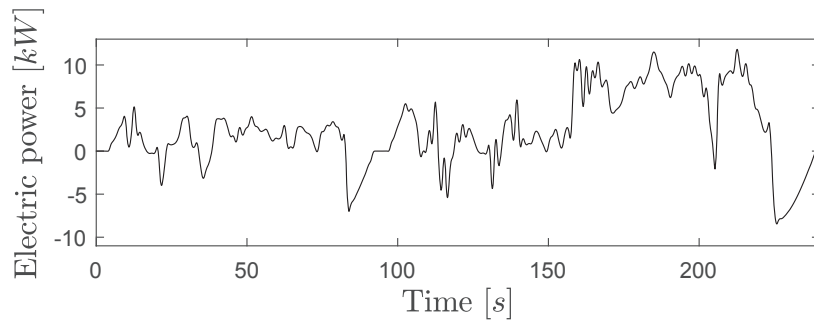
**TABLE 1** Parameters of the simulated 10kW Fuel Cell Module (FCM).

PS-FBC parameters				FC parameters			
$L_f$	$6\mu H$	$R_0$	$100m\Omega$	$N_{stack}$	55	$E_{nl}$	$0.95V$
$C_f$	$1550\mu F$	$n$	20	$r_{ohm}$	$0.5m\Omega$	$A_t$	$45.56mV$
$R_f$	$5m\Omega$	$V_{bus}$	$400V$	$m$	$2mV$	$n$	$0.008\frac{1}{A}$
$L_0$	$1000\mu H$	$f_s$	$30kHz$	$C_{dl}$	$4.9F$		

STA parameters				ESS parameters <sup>37</sup>			
$\alpha$	0.14	$C$	$3.00e^5 kW/s$	$V_{sc}^n$	$48V$	$R_{sc,s}$	$10m\Omega$
$\lambda$	$4.8e^{-4}$	$K_m$	$2.50e^5 kW/s$	$C_{sc}$	$83F$	$R_{sc,p}$	$16k\Omega$
		$K_M$	$3.75e^5 kW/s$	$L_{sc}$	$30\mu H$	$C_{bus}$	$500\mu F$

To evaluate the FCM control, the HPS is assumed to operate under highly variable power demand  $p_L$ . The power profile was generated in accordance with the EPA IM240 driving urban cycle, considering a 400kg electric vehicle (see Fig. 9). Additionally, the poorly regulated bus voltage  $v_{bus}$  is shown in Fig. 10. As previously stated, to test the robustness of the SOSM-STA controller, voltage disturbances of 5% have been allowed.



**FIGURE 9** Load power profile  $p_L$  generated from the EPA IM240 driving urban cycle.

To safeguard the FC lifetime, the smooth FCM power reference  $p_{0r}$  was generated by means of a typical frequency decouple strategy<sup>30</sup>, with a cut-off frequency of  $0.1Hz$  (see Fig. 11). Note that, as it was explained, the difference between load power  $p_L$  and FCM output power  $p_0$  is provided by the ESS.

The Fig. 11 presents time response of designed SOSM-STA control system. In addition to the proposed controller, a conventional First Order SMC (FO-SMC) is also shown to compare their performance. The FO-SMC is designed in accordance to the system perturbation and uncertainties considered for the STA analysis (see Appendix B).

As it can be appreciated, both controllers achieve robust tracking for the FCM power output,  $p_{0r}$ , in spite of variable power demand, disturbed  $v_{bus}$  and system uncertainties. Nevertheless, the Super-Twisting Algorithm achieves a considerable amelioration of chattering, leading to an important control effort reduction. For illustrative purposes, the zoom in the figure portrays the chattering of the proposed controller in the neighborhood of the nominal power, showing that it is lowered to approximately

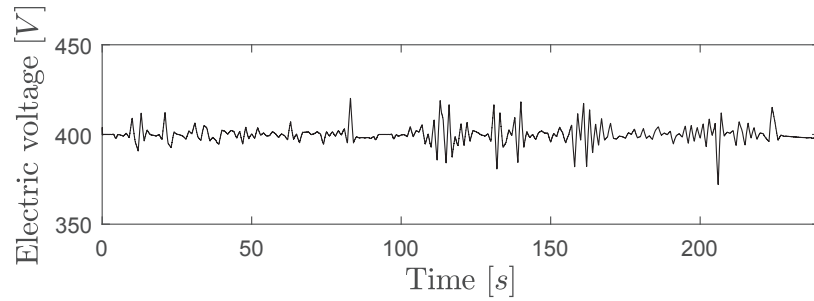


**FIGURE 10** Time response of the perturbed bus voltage  $v_{bus}$ .

25% of the FO-SMC chattering. In addition, a reduction of  $p_0$  chattering basically results in lesser current chattering through the FCM and, consequently, power losses diminution, so overall efficiency is enlarged.

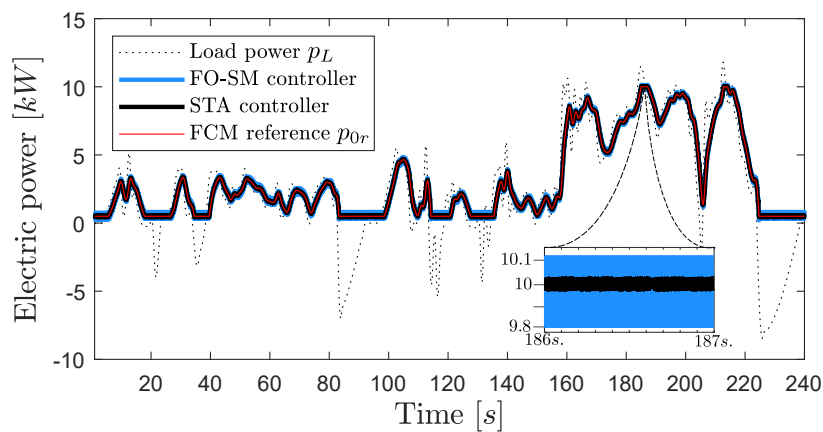


**FIGURE 11** Control system tracking of the FCM power reference  $p_{0r}$ .

The evolution of  $\sigma$  and  $\dot{\sigma}$  is presented in Fig. 12, when the system has already reached the sliding manifold  $S$ . It can be observed that, once the system is led onto  $S$  by the proposed SOSM-STA controller, it never leaves the sliding manifold, ensuring its robust permanency and, therefore, guaranteeing the tracking of the power reference  $p_{0r}$ . The detail shows the smooth variation of the STA which is responsible of the chattering reduction, with respect to the conventional SMC.

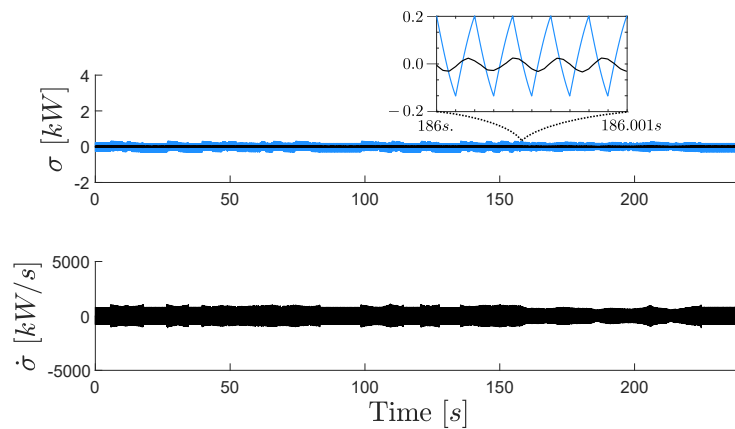


**FIGURE 12** Time response of sliding variable  $\sigma$  and  $\dot{\sigma}$ .

The Fig. 13 shows the stable response of the zero dynamics states,  $v_f$  and  $i_f$ . As it can be appreciated, the stability region, computed by the analysis described in Sec. 4, settles upper and lower bounds for the voltage variations of the input filter. Inside this stable region, which is defined through the proper selection of the filter elements, the secure operation of the fuel cell is guaranteed and the desired performance of the overall control system is assured.

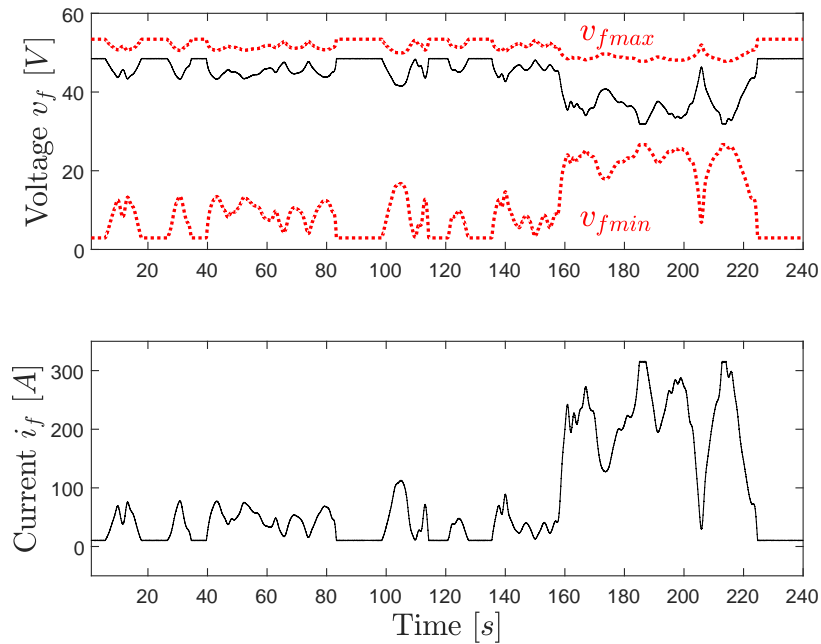


**FIGURE 13** Stable response of zero dynamics states  $v_f$  and  $i_f$ .

## 6 | CONCLUSION

This paper proposed a power tracking SM controller for a PS-FBC based Fuel Cell Module. This PS-FBC based topology provides high conversion ratio through its high frequency transformer, which is required to deal with the low output voltage of the FC. This feature prevents the converter from operating with a large duty cycle and reduces system losses, allowing its application in medium power systems.

To reduce output chattering, typical in several SMC systems, a continuous SOSM controller based on a Super-Twisting Algorithm was developed. The proposed controller proves to successfully attain robust tracking of the power reference, in spite of variable power demand, voltage bus variations and system parameters uncertainties.

To guarantee the stability of the controlled system on the sliding manifold  $\mathcal{S}$ , the Zero Dynamics were analysed. Due to ZD structure, standard Lyapunov functions were not applicable. To overcome this drawback, a diffeomorphism was used to bring the dynamics into a Lienard-type form, allowing the utilization of a special integral Lyapunov function.

Finally, it can be remarked that the designed Super-Twisting controller has low computational complexity, a very important feature for implementation. Additionally, the resulting Fuel Cell Module is highly versatile, i.e. it is not restricted to a particular hybrid systems, but instead it is feasible to be integrated into different topologies composed of diverse alternative sources/storage devices.

The forthcoming phase of this project is twofold. On the one hand, efforts will be focused on experimentally validating the satisfactory simulation results in an actual fuel cell-based hybrid testbench. On the other, theoretical development will be undertaken to improve the proposed Super Twisting controller, particularly aiming to design an adaptive gain STA set-ups capable to further reduce the control effort and chattering.

## ACKNOWLEDGMENTS

This research was supported by the Universidad Nacional de La Plata, the Consejo Nacional de Investigaciones Científicas y Técnicas (CONICET) and the Agencia Nacional de Promoción Científica y Tecnológica (ANPCyT) from Argentina.

## References

1. Lai J, Ellis MW. Fuel Cell Power Systems and Applications. *Proceedings of the IEEE* 2017; 105(11): 2166-2190.
2. Patterson M, Macia NF, Kannan AM. Hybrid Microgrid Model Based on Solar Photovoltaic Battery Fuel Cell System for Intermittent Load Applications. *IEEE Transactions on Energy Conversion* 2015; 30(1): 359-366.
3. Tran VL, Tran NT, Yu SH, Park Y, Choi W. Design of a Nonisolated Fuel Cell Boost Charger for Lithium Polymer Batteries With a Low Output Ripple. *IEEE Transactions on Energy Conversion* 2015; 30(2): 605-614.
4. Wang Y, Chen K, Mishler J, Chan Cho S, Cordobes Adroher X. A review of polymer electrolyte membrane fuel cells: Technology, applications, and needs on fundamental research. *Applied Energy* 2011; 88(4): 981-1007.
5. Thounthong P, Rael S, Davat B. Analysis of Supercapacitor as Second Source Based on Fuel Cell Power Generation. *IEEE Transactions on Energy Conversion* 2009; 24(1): 247-255.
6. Hajizadeh A, Golkar MA, Feliachi A. Voltage Control and Active Power Management of Hybrid Fuel-Cell/Energy-Storage Power Conversion System Under Unbalanced Voltage Sag Conditions. *IEEE Transactions on Energy Conversion* 2010; 25(4): 1195-1208.
7. Abkenar AT, Nazari A, Jayasinghe SDG, Kapoor A, Negnevitsky M. Fuel Cell Power Management Using Genetic Expression Programming in All-Electric Ships. *IEEE Transactions on Energy Conversion* 2017; 32(2): 779-787.
8. Ouyang Z, Andersen MAE. Overview of Planar Magnetic Technology - Fundamental Properties. *IEEE Transactions on Power Electronics* 2014; 29(9): 4888-4900.
9. Magambo JSNT, Bakri R, Margueron X, et al. Planar Magnetic Components in More Electric Aircraft: Review of Technology and Key Parameters for DC-DC Power Electronic Converter. *IEEE Transactions on Transportation Electrification* 2017; 3(4): 831-842.
10. Kolli A, Gaillarda A, De Bernardinis A, Bethoux O, Hissela D, Khatir Z. A review on DC/DC converter architectures for power fuel cell applications. *Energy Conversion and Management* 2015; 105: 716-730.
11. Xinbo R. *Soft-Switching PWM Full-Bridge Converters: Topologies, Control and Design*. Wiley . 2014.
12. Kunusch C, Puleston P, Mayosky M. *Sliding-Mode Control of PEM Fuel Cells*. Springer London . 2012.
13. Shams-Ansari A, Razavi F, Ghadimi A, Abolmasoumi H. Implementation of Sliding Mode Control in a Full Bridge (DC-DC) Converter. *Indian Journal of Science and Technology* 2012; 5: 2665-2672.
14. Senapati R, Sahoo R, Senapati R, P. P. Design and analysis of Sliding Mode Controller for Isolated Full Bridge DC-DC converter. *1st IEEE International Conference on Power Electronics, Intelligent Control and Energy Systems (ICPEICES-2016)* 2016.
15. Fridman L, Moreno J, Bandyopadhyay B, Kamal S, Chalanga A. *Continuous Nested Algorithms : The Fifth Generation of Sliding Mode Controllers* ch. 1; Springer International Publishing . 2015.
16. Fridman L, Moreno J, Iriarte R. *Sliding Modes after the first Decade of the 21st. Century*. Springer . 2011.
17. Bandyopadhyay B, Sivaramakrishnan J, Spurgeon S. *Advances in sliding mode control. Concept, theory and implementation..* 440. Springer . 2013.

18. Fridman L, Barbot JP, Plestan F. *Recent Trends in Sliding Mode Control*. IET . 2016.
19. Li S, Yu X, Fridman L, Man Z, Wang X. *Advances in Variable Structure Systems and Sliding Mode Control - Theory and Applications*. 115. Springer . 2018.
20. Singh S, Gautam A, Fulwani D. Constant power loads and their effects in DC distributed power systems: A review. *Renewable and Sustainable Energy Reviews* 2017; 72: 407-421.
21. Alexey S. and Juan E. Machado and Romeo Ortega and Johannes Schiffer and Anton A. Pyrkin . On the Existence and Long-Term Stability of Voltage Equilibria in Power Systems with Constant Power Loads. *CoRR* 2018; abs/1809.08127.
22. Liu J, Zhang W, Rizzoni G. Robust Stability Analysis of DC Microgrids With Constant Power Loads. *IEEE Transactions on Power Systems* 2018; 33(1): 851-860.
23. Wu J, Lu Y. Adaptive Backstepping Sliding Mode Control for Boost Converter With Constant Power Load. *IEEE Access* 2019; 7: 50797-50807.
24. Larminie J, Dicks A. *Fuel Cell Systems Explained*. Wiley. 2nd ed. 2003.
25. Benmouna A, Becherif M, Depernet D, Ebrahim MA. Novel Energy Management Technique for Hybrid Electric Vehicle via Interconnection and Damping Assignment Passivity Based Control. *Renewable Energy* 2018; 119: 116 - 128.
26. O. Kraa and H. Ghodbane and R.Saadi and M.Y. Ayad and M. Becherif and A. Aboubou and M. Bahri . Energy Management of Fuel Cell/ Supercapacitor Hybrid Source Based on Linear and Sliding Mode Control. *Energy Procedia* 2015; 74: 1258 - 1264. The International Conference on Technologies and Materials for Renewable Energy, Environment and Sustainability –TMREES15.
27. Moré J, Puleston P, Kunusch C, Fossas E. Multi Input Sliding Mode Control of an Autonomous Fuel Cell-Supercapacitor Hybrid System. *12th IEEE Workshop on Variable Structure Systems*, 2012.
28. Ghadimi A, Rastegar H, Keyhani A. Development of Average Model for Control of a Full Bridge PWM DC-DC Converter. *Journal of Iranian Association of Electrical and Electronics Engineers* 2007; 14.
29. Moré JJ, Puleston PF, Kunusch C, Fantova MA. Development and Implementation of a Supervisor Strategy and Sliding Mode Control Setup for Fuel-Cell-Based Hybrid Generation Systems. *IEEE Transactions on Energy Conversion* 2015; 30(1): 218–225.
30. Snoussi J, Benelghali S, Benbouzid M, Mimouni M. Optimal sizing of energy storage systems using frequency-separation-based energy management for fuel cell hybrid electric vehicles. *IEEE Transactions on Vehicular Technology* 2018; 67: 9337-9346.
31. Levant A. Principles of 2-sliding mode design. *Automatica* 2007; 43(4): 576 - 586.
32. Shtessel Y, Edwards C, Fridman L, Levant A. *Sliding Mode Control and Observation*. Springer New York . 2014.
33. Miyagi H, Munda JL, Miyagi N. Study on Lyapunov Functions for Lienard-type Nonlinear Systems. *IEEJ Transactions on Electronics, Information and Systems* 2001; 121(4): 748-755.
34. Utkin V. *Sliding Modes in Control and Optimization*. Communication and control engineering series Springer-Verlag . 1992.
35. San Martín I, Ursúa A, Sanchis P. Modelling of PEM Fuel Cell Performance: Steady-State and Dynamic Experimental Validation. *Energies* 2014; 7: 670-700.
36. Ballard Power System, Inc. . FCvelocity – 9SSL- Ballard Power. tech. rep., Ballard; <http://www.ballard.com>: 2011.
37. Maxwell Technologies, Inc. . Datasheet - 48V Modules. Tech. Rep. 1009365.13, ; <https://www.maxwell.com/>: 2013.



**How to cite this article:** Anderson J.L., Moré J.J., Puleston P.F. (2019), Design and Stability Analysis of a Super-Twisting Controller for a PS-FBC based Fuel Cell Module

## APPENDIX

### A SUPERCAPACITOR BASED ENERGY STORAGE SYSTEM MODULE

The control parameters of the ESS module, employed in the simulation results, are detailed in Table A1. To regulate the bus voltage, a typical nested PI controller setup applied to a boost converter (see Fig. A1) was taken into account, achieving an overshoot of less than 5% and a settling time of 10ms at nominal conditions.

**TABLE A1** Control parameters of the ESS.

External loop		Internal loop	
$Ki_v$	9.86	$Ki_i$	1.29
$Kp_v$	0.326	$Kp_i$	$0.452e^{-3}$

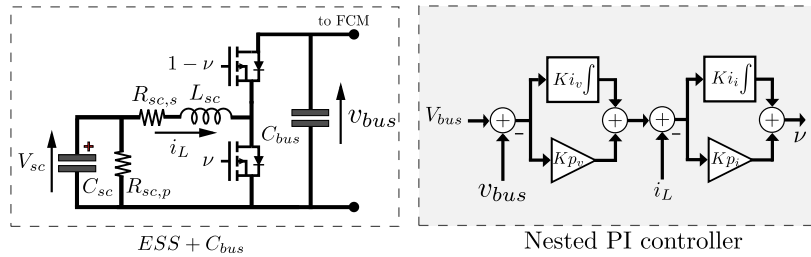


**FIGURE A1** Schematic diagram of the ESS topology and controller based on a nested PI controller.

### B FIRST ORDER SLIDING MODE CONTROLLER

In order to reduce control chattering and achieve a valid comparison for the proposed SOSM-STA controller, a two term controller based on conventional SMC is designed, as well as in (17), i.e.

$$u_{(x,t)} = u_{ff(x,t)} + u_{smc(x,t)}, \quad (\text{B1})$$

where  $u_{ff}$  is equal to (18) and  $u_{smc}$  is a conventional SMC equals to:

$$u_{smc(x,t)} = -k \cdot \text{sign}(\sigma_{(x,t)}), \quad \text{with } k = 0.015. \quad (\text{B2})$$